

Unbiased Clustering of Residues Undergoing Synchronous Motions in Proteins using NMR Spin Relaxation Data

V. S. Manu¹, Giuseppe Melacini,² Evgenii L. Kovrigin,⁵ J. Patrick Loria,^{3,4} and Gianluigi Veglia^{1,4}*

¹Department of Biochemistry, Molecular Biology, & Biophysics – University of Minnesota, Minneapolis, MN 55455.

²Department of Chemistry and Chemical Biology & Department of Biochemistry and Biomedical Sciences, McMaster University, Hamilton, ON, Canada.

³Department of Chemistry, Yale University, New Haven, CT, United States.

⁴Department of Molecular Biophysics and Biochemistry, Yale University, New Haven, CT, United States

⁵Department of Chemistry and Biochemistry, University of Notre Dame, Notre Dame, IN, United States

***Corresponding Author**

Gianluigi Veglia
Department of Chemistry and Department of Biochemistry,
Molecular Biology, and Biophysics,
312 Church St. SE, Minneapolis, MN 55455
Telephone: (612) 625-0758
Fax: (612) 625-5780E-mail: veqli001@umn.edu.

ABSTRACT

Biological macromolecules are dynamic entities that transition between various conformational states, often playing a vital role in biological functions. Their inherent flexibility spans a broad range of timescales. Motions occurring within the microsecond to millisecond range are especially important, as they are integral to processes such as enzyme catalysis, folding, ligand binding, and allostery. NMR Carr-Purcell-Meiboom-Gill (CPMG) relaxation dispersion measurements are the preferred method for characterizing macromolecular motions at atomic resolution. However, it is still uncertain whether the functional motions of multiple residues in macromolecules need to be coordinated and/or synchronized within the protein matrix in order to perform the desired function. Here, we illustrate an unbiased method to analyze NMR relaxation dispersion and identify dynamic clusters of residues that fluctuate on similar timescales within proteins. The method requires relaxation dispersion data for backbone amides or side-chain methyl groups, which are globally fitted using the Bloch-McConnell equations for each pair of residues. The goodness of the pairwise fitting serves as a metric to construct two-dimensional synchronous dynamics (SyncDyn) maps, allowing us to identify residue clusters whose dynamics are influenced by ligand binding. We applied our method to the catalytic subunit of the cAMP-dependent protein kinase A (PKA-C) and the T17A mutant of ribonuclease A (RNase A). The SyncDyn maps for PKA-C showed distinct clusters of residues located in critical allosteric sites. Nucleotide binding activates the movement of residues at the interface between the two lobes and also those distal to the active site. In the case of RNase A, the SyncDyn maps show that residues fluctuating with the same time scale are interspersed in both lobes of the enzyme. Overall, our approach eliminates arbitrary manual selection of residues for dynamic clustering and objectively identifies all possible residue pairs that fluctuate synchronously, i.e. on the same timescale.

Keywords: NMR dynamics, CPMG, relaxation dispersion curves, synchronous motion, protein kinase A, RNase A.

INTRODUCTION

Many proteins experience widespread molecular motions that occur on the μs - ms timescale that are important for their function.[1-5] These motions can include protein sub-domains, active site loops, and folding-unfolding transitions.[6] In addition, the phenomenon of allostery [7, 8] that relays signals between two distinct protein sites (classically, ligand binding sites) often relies on networks of flexible amino acid residues to enable this communication.[9-13] Specific examples include disease-causing mutations that can alter the biological function of proteins and enzymes by disrupting the necessary global motions.[10, 14] Despite the biological importance and sustained study a unified mechanistic description of how allosteric signals are relayed through the protein matrix remains in flux and is likely dissimilar for different proteins.[15]

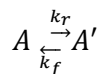
One experimental method that can characterize molecular motions and their role in conformational changes and allostery is solution NMR spectroscopy. Solution NMR spectroscopy can directly detect subtle, atomic-level structural and dynamical perturbations that mediate conformational changes including allosteric processes.[16-19] These structural fluctuations can be detected using Carr-Purcell-Meiboom-Gill (CPMG) relaxation dispersion experiments, [20, 21] which provide residue-specific relaxation dispersion curves that are used to quantify kinetics (exchange constant, k_{ex}) and thermodynamic (populations, p_A and p_A') parameters for exchange processes occurring on the μs - ms timescale.[3] The residue-specific nature of the information obtained from relaxation dispersion experiments also presents problems in interpretation. One would like to know whether multiple residues are moving together (in concert) or independently. Historically, this was assessed by comparing k_{ex} values and using some (often arbitrary) criteria, *i.e.*, determining whether k_{ex} values are similar enough to warrant grouping into a single motional process. Furthermore, when many residues show promising relaxation dispersion curves, grouping them by similar k_{ex} values is a difficult task and often very tedious to perform manually. Typically, dynamic parameters are determined for individual sites with high precision and then compared to

suggest potential correlations. However, such manual analysis is prone to bias of the individual researcher.

Here, we propose an alternative method to automatically cluster residues undergoing synchronous motions (*motions with the same k_{ex} values and populations*) in proteins. This method builds upon a previous approach we described to identify the collective dynamic response for the catalytic subunit of the cAMP-dependent protein kinase A (PKA-C) to ligand binding.[22] In this revised method, we fit the CPMG relaxation dispersion data (either backbone amides or side-chain methyl groups) for each residue pair in the protein using the Bloch-McConnell equations, [23] and utilize the goodness of the pairwise fitting as a metric to build two-dimensional dynamic correlation (SyncDyn) maps and cluster residues whose motions are fluctuating synchronously. We applied our method to two proteins with well-characterized millisecond motions, PKA-C in different ligated forms and the T17A mutant of the ribonuclease A (RNase A). We show how ligand binding or single mutations modulate the organization of the internal dynamic network of these enzymes.

THEORY AND DATA ANALYSIS

To fit the CPMG dispersion curves, we consider a single residue undergoing a two-site exchange between a ground (A) and higher energy (A') state:



where k_f and k_r are the forward and reverse rate constants of the exchange process, respectively.

The evolution of the magnetization for this system can be written as

$$\frac{d}{dt} \begin{bmatrix} M_A \\ M_{A'} \end{bmatrix} = \begin{bmatrix} -R_{2A}^0 - k_f & k_r \\ k_f & -R_{2A'}^0 - k_r + i\Delta\omega \end{bmatrix} \begin{bmatrix} M_A^0 \\ M_{A'}^0 \end{bmatrix} \quad (1)$$

where M_A and $M_{A'}$ are the transverse magnetizations for A and A', respectively, R_{2A}^0 and $R_{2A'}^0$ are the intrinsic transverse relaxation rates for A and A', and $\Delta\omega$ is the chemical shift difference between sites A and A' expressed in angular frequency units (s^{-1}). If $\rho_A \gg \rho_{A'}$ and we if we also assume that $R_{2A}^0 = R_{2A'}^0 = R_2^0$, the solution of equation (1) is

$$\begin{bmatrix} M_A \\ M_{A'} \end{bmatrix} = \exp\left(\begin{bmatrix} -R_2^0 - k_f & k_r \\ k_f & -R_2^0 - k_r + i\Delta\omega \end{bmatrix} t\right) \begin{bmatrix} M_A^0 \\ M_{A'}^0 \end{bmatrix} \quad (2)$$

For the constant relaxation time CPMG relaxation dispersion (RD) experiment, the transverse relaxation rates ($R_{2,Eff}$) are determined from the observed resonance intensities using the following expression:

$$R_{2,Eff} = \frac{-1}{T_{CPMG}} \ln\left(\frac{I_A}{I_A^0}\right) \quad (3)$$

where T_{CPMG} is the total CPMG relaxation delay, I_A is the observed peak intensity after the CPMG sequence ($T_{CPMG} \neq 0$) and I_A^0 is the intensity of the reference spectrum ($T_{CPMG} = 0$). The RD profile results from a series of $R_{2,Eff}$ at different values as a function of the π pulse frequency (ν_{CPMG}) where $\nu_{CPMG} = 1/(2\tau_{CPMG})$, in which τ_{CPMG} is the time interval between 180° pulses in the CPMG element. To construct the SyncDyn map, we begin with equation (3) and use the following steps:

Step 1. $R_{2,Eff}$ calculation for individual residues. After collecting the CPMG RD data at a single or multiple \mathbf{B}_0 fields, we calculate the $R_{2,Eff}$ values using equation 3 for different ν_{CPMG} values.

Step 2. Identification of all residue pairs. We identify all non-equivalent residues pairs, which are $N \times (N - 1) / 2$ where N is the number residues in the protein.

Step 3. Pairwise fitting of all RD profiles. For a pair of protein residues, i and j , the two RD profiles at a single \mathbf{B}_0 field, RD^i and RD^j , depend on $k_f^i, k_r^i, R_2^{0i}, \Delta\omega^i$ and $k_f^j, k_r^j, R_2^{0j}, \Delta\omega^j$,

respectively. To fit the RD profiles of the residue pair simultaneously, we assume that the kinetic constants, k_f and k_r , are the same for both residues:

$$k_f^i = k_f^j = k_f \quad (4)$$

$$k_r^i = k_r^j = k_r \quad (5)$$

Therefore, RD^i and RD^j can be fitted using the Bloch-McConnell equation, combining all the parameters, $k_f, k_r, R_2^0, R_2^j, \Delta\omega^i, \Delta\omega^j$, into a single set. The resulting fitted RD profiles, RD_{fit}^i and RD_{fit}^j , are then used to assess the goodness of the fit with the experimental RD data for residues i and j .

Step 4. Calculating the goodness of the pairwise fitting using R-squared. To assess the goodness of the pairwise fitting, we utilized the R-squared value between the experimental and fitted RD profiles using the following equation [24]:

$$(R - \text{squared})_{i,j} = 1 - \frac{SSR}{SST} \quad (6)$$

Where

$$SSR = \sum_{k=1}^n ([RD_k^i, RD_k^j] - [RD_{fit,k}^i, RD_{fit,k}^j])^2 \quad (7)$$

and

$$SST = \sum_{k=1}^n ([RD_k^i, RD_k^j] - [\overline{RD^i}, \overline{RD^j}])^2 \quad (8)$$

$$\overline{RD^i} = \frac{1}{n} \sum_{k=1}^n RD_k^i \quad (9)$$

SSR is the regression sum-of-squares and SST total sum-of-squares, n is the number of v_{CPMG} points, RD and RD_{fit} are experimental and fitted dispersion profiles. We calculated the R-squared values for each residue across the various B_0 fields and identified the minimum R-squared value

among all the dispersion curves and all residue pairs. The R-squared ranges from 0 to 1. A high R-squared value for a residue pair indicates that the initial assumption is highly probable, *i.e.*, the residues are likely to exchange between two states with similar frequency. A low value of R-squared indicates that the motions of the two residues occur on a different timescale (**Fig.1**). The final SyncDyn map consists of a matrix of R-squared values, where each element (i, j) represents the R-squared value between the residue pairs.

To validate this approach, we considered two residues, X and Y, exchanging with their respective minor states X' and Y'. We simulated two hundred synthetic CPMG dispersion curves for X, assuming exchange rates ranging between 0 and 5000 s⁻¹. For each dispersion curve of X, we simulated 120 CPMG dispersion curves for residue Y. The exchange rate of Y was selected in such a way that the difference in k_{ex} between X and Y would vary uniformly from 0 to 3000 s⁻¹. The population of X' and Y' were assumed to be 0.02 for all the simulations (**Fig.2**).

We then calculated the pairwise R-squared values for the 200 x 120 pairs and plotted as a function of the exchange rate for X (k_{ex}^X) on the horizontal axis and the difference between the exchange rates of X and Y ($\Delta k_{ex} = k_{ex}^X - k_{ex}^Y$) on the vertical axis (**Fig.2**). We found that the R-squared values decrease with increasing Δk_{ex} , with the most reliable correlations occurring for exchange kinetics between 200 and 4000 s⁻¹, as expected for typical CPMG experiments.[3] On the other hand, faster exchange rates give rise to flat dispersion profiles, which may result in artifactual correlations in the SyncDyn maps, especially in the presence of experimental noise. To test this, we compared two simulated sets of data using random noise of 2 and 5% (**Fig.2a** and **2b**). We found that as the noise amplitude increases, the R-squared values significantly decrease, indicating that for reliable correlations it is critical to have high-quality relaxation dispersion data with low noise levels, especially for exchange rates near the fast limit as suggested previously [25].

Validation of the protocol using a synthetic CPMG dataset. To test our clustering algorithm, we simulated a set of synthetic CPMG data for a hypothetical twenty amino acid peptide with two clusters of three residues, *i.e.*, cluster 1 with k_f and k_r of 25 and 500 s^{-1} , and cluster 2 with k_f and k_r of 100 and 2000 s^{-1} (**Fig.3a**). As shown in **Fig.3b**, our algorithm identifies the correlations between the two clusters of residues that share similar exchange kinetics as indicated by the off-diagonal elements in the 2D SyncDyn map and illustrated in the dendrogram (**Fig.3c**).

RESULTS

We applied our approach to analyze two dynamic enzymes (**Fig.S1**), PKA-C and RNase A. PKA-C is a ubiquitous kinase responsible for phosphorylating numerous cell substrates,[26, 27] while RNase A catalyzes the transphosphorylation and hydrolysis of single-stranded RNA.[28] Both enzymes exhibit critical conformational fluctuations in the millisecond time scale during their catalytic cycles. We reevaluated their NMR relaxation dispersion data to identify potential clusters of residues that undergo synchronous motions.

Clustering synchronous residues of PKA-C. We first examined the CPMG relaxation dispersion data for the methyl group of the aliphatic side chains of PKA-C.[22, 29-31] This bilobate enzyme undergoes open-to-close transitions through its catalytic cycle.[32] The apo enzyme binds the nucleotide and adopts a partially closed conformation with a higher affinity for the substrate (positive cooperativity).[33] After substrate binding, the chemical step (phosphoryl transfer) is relatively fast (500 s^{-1}), and the product release constitutes the rate-determining step of the catalytic cycle.[34-36] We previously found that synchronous and asynchronous fluctuations are hallmarks for the formation of the dynamically committed state and for product release, respectively. [22, 36] The motions of this enzyme are exquisitely tuned to kinase function, as allosteric mutations of PKA-C within the substrate recognition sequence affect the enzyme's opening and

closing kinetics, influencing its catalytic efficiency [56-58], while the binding of inhibitors quenches the motions in the μs -ms time scale.[33, 35]

The SyncDyn map of the apoenzyme shows that the μs -ms motions are located into two separate clusters, spanning residues 5 – 100 and 150 – 200 (**Fig.4a** and **Fig.S2**). Additionally, the SyncDyn map displays a few correlations among residues at the C-terminal tail, which wraps around the two lobes, and these two well-defined dynamic clusters.

A closer inspection of the overall and range-specific SyncDyn maps reveals that the apo enzyme displays residues spanning from the small to the large lobe, *i.e.*, V57, L82, I94, L95, L103, V104, I150, and L172 (**Figs.S2a-b**). Among those residues, V57 is part of the kinase's C spine, a continuous array of hydrophobic residues necessary for its activation.[37, 38] L103 and V104 bridge the C spine with the regulatory (R) spine, formed upon phosphorylation of the activation segment. I150 is another essential residue within the core of the enzyme, and when mutated into alanine, PKA-C does not undergo autophosphorylation at T197 and S338, rendering the enzyme inactive.[31]SyncDynSyncDyn

Upon nucleotide binding, the density of the R-squared correlations from residue 50 to 200 increases, which is consistent with the structural and dynamic role of the nucleotide acting as an allosteric effector.[37, 38] Notably, the distribution of the exchange rates changes from an average of 800 to 2000 s^{-1} , suggesting that the $\text{ATP}_{\gamma}\text{N}$ binding shifts the frequency of the opening and closing of the enzyme's active site (**Figs.4a-b**). Of note, this change in motion corresponds to an increase of binding affinity between the kinase substrates or pseudo-substrate inhibitor PKI.[33] The SyncDyn map, along with the residues mapped onto the X-ray structures (**Figs.4, S2, and S3**), indicates that the two dynamic clusters of the apo kinase become interconnected upon nucleotide binding. Synchronous motions involve the hydrophobic core of the kinase, especially L172 (C spine), V182, I174, I150, and I180. Notably, a single mutation in this cluster (*i.e.*, I150A)

completely disrupts kinase's activity.[31] Motions in the same timescale is identified for residues that bridge the α E-helix in the C-lobe and the α C-helix in the N-lobe, including I94, L160, L162, and L157. The network of synchronous residues crosses the enzyme's structure horizontally, at the hydrophobic interface between the two lobes harboring the substrate binding pocket and radiates to the small lobe via the hydrophobic spines.(**Fig.S5**) Residues linking the B and C helices also fluctuates in a similar time scale, which agrees with the critical role of these segments in assembling the kinase's active conformation.[32]

We then tested the two inhibited forms of the kinase. Both inhibitors quenched the internal dynamics in the μ s-ms time scale.[39] For both ligated forms of PKA-C, we observe a partial (balanol) and a complete (H89) disruption of the dynamic networks, showing that the change in frequency of the enzyme's fluctuations may affect its affinity for substrate binding (**Fig.4**). The populations of the conformationally excited states as determined from the fitting of the CPMG relaxation dispersion curves are summarized for all the kinase forms in **Fig.S4** and reflect the dynamic activation of the nucleotide and the suppression of the conformationally excited states by balanol,[39] a phenomenon previously observed in the catabolite activator protein.[40] Note that out of the 102 methyl probes assigned and analyzed with SyncDyn and using the GUARD software,[41] eleven residues could not be fitted using a two-state model and are consequently omitted from the SyncDyn plots These residues are distributed throughout the enzyme and are illustrated in **Fig.S6**. Additional experiments at various field strengths will be necessary to accurately quantify the kinetics and populations of these residues, a task that lies beyond the scope of this study.

Overall, the SyncDyn maps highlighted the clusters of residues that fluctuate at the same frequency both in the free and ligated forms. This information is complementary to the CHESCA maps,[22] and provide a starting point to interrogate the allosteric phenomena occurring within the kinase upon ligand binding and mutations.[42-44]

Analysis of the slow motions in the T17A mutant of RNase A. As a second example, we applied our analysis method to the ^{15}N -CPMG relaxation dispersion data set available for RNase A. This well-studied enzyme catalyzes the cleavage of single-stranded RNA without metals or co-factors. The RNase A architecture consists of three α -helices and seven β -strands organized into two lobes with the active site positioned between the lobes (**Fig.S1b**). Motions play a significant role in the catalytic cycle of RNase A as the rate-determining step (product release) is coupled with a conformational change involving residues throughout the entire protein structure. [45-47] NMR relaxation dispersion data revealed that the residues of the RNase can be grouped into two dynamic clusters. [48-50] Specifically, loops 1 and 4 positioned at ~ 20 Å away from the active site impart substrate fidelity, recognizing purine residues at the 5' end of the phosphoester cleavage site (**Fig.S1b**). These loops undergo a conformational change of 2-3 Å upon ligand binding, defining the closed state of the enzyme. After the chemical step, RNaseA requires an additional conformational change on the millisecond timescale for product release. Mutagenesis and structural dynamic studies have shown that the H48 side chain forms critical H-bond interactions with the surrounding residues affecting the motions of remote structural elements, such as loops 1, α -helices 1 and 2, as well as β 1, β 2, and β 4 strands (**Fig.S1b**). In particular, the H48A mutation disrupts these H-bond interactions dramatically affecting the enzyme's activity. In contrast, mutations at T17 (also involved in H-bond interactions) slightly accelerate the product off rate by increasing the motion of loop 1. [49] Because of the extensive data available for this mutant, we chose it for our SyncDyn analysis. The SyncDyn map generated with these data and the distribution of the k_{ex} values are reported in **Figs.5a-b and Fig.S7**. The SyncDyn map shows that several residues intersperse throughout the protein experience a motion in the same timescale, *i.e.*, residues located around loop 4 connecting strands 2 and 3 (A64, Q69, T70, and N71). These residues fluctuate in the same timescale as those belonging to the adjacent β -strand and distal residues located in the β -hairpin connecting strands 4 and 5 and helices 1 and 2. Finally, C95

fluctuates with a k_{ex} similar to residues located in the opposite dynamic cluster, *i.e.*, I106, A109, E111, H119, and S123. Note that the comprehensive SyncDyn map contains the information for a broad range of k_{ex} , spanning from 0 to 5000 s^{-1} . However, the distribution of the k_{ex} values indicates that structural fluctuations with R-squared of 0.85 occur between 0 and 5000 s^{-1} (**Fig.5b**), with most of the fluctuations occurring around 3000 s^{-1} , while only a few residues fluctuate at frequencies between 0 – 1000 and 4000 – 5000 s^{-1} range. Overall, the SyncDyn map for RNase A shows that many residues belonging to the two dynamic clusters move synchronously. However, it should be noted that the motions between the two lobes of the enzyme are not coupled, although the fluctuation of the individual residues occurs in the same time scale [50].

DISCUSSION

Synchronous motions have been suggested to favor allosteric transmission from the ligand-binding site to remote sites of proteins.[51] Recent studies also infer that these structural fluctuations must be correlated and occur within a defined frequency range to modulate allosteric phenomena efficiently.[52, 53] NMR studies of various enzymes have shown that V-type and K-type allosteric enzymes' regulation occurs in the μs -ms time scale, [1, 2, 54-57] a window of motions exquisitely captured by the CPMG dispersion experiments.[3, 58-60] The dispersion data obtained from CPMG experiments at multiple frequencies are used to extract kinetic and thermodynamic parameters on the conformational equilibrium of biomacromolecules. The most common analysis method involves a global fitting of the flexible residues using the Bloch-McConnell equations under the assumption of a two-site exchange equilibrium.[23] When a global k_{ex} is obtained, subsets of residues are selected to identify clusters of residues that fluctuate at a similar frequency and may be involved in allosteric networks. The latter comes at the expense of the accuracy of individual curve fitting. [61] In contrast, our method utilizes a geometrical approach to evaluate pairwise synchronicity by measuring the distance between residues in the k_f/k_r space. If residues share similar kinetic parameters, they cluster in the k_f/k_r space, displaying correlations in a 2D

SyncDyn map. Although computationally demanding, this method does not rely on an arbitrary selection of residues as it systematically analyzes all residue pairs, and it objectively provides a more accurate fit of individual dispersion curves than the standard global fitting approach.

As expected, we found that pairwise dynamic correlations critically depend on the quality of the relaxation dispersion data. Specifically, spectral noise levels may cause false positives (or negatives) that affect the fidelity of the SyncDyn maps. To avoid this, the new algorithm utilizes pair-fitting procedures stricter than individual fitting, and the goodness of fit (R - squared) avoids the overestimation of pairwise correlations. *Note that our method only clusters residues that fluctuate at similar frequencies (k_f and k_r) and does not identify whether these fluctuations are coupled or correlated (e.g., RNase A).* Indeed correlated motions have been proposed to be a critical property of allosteric proteins [62]; however, determining whether motions are correlated requires the support of computational approaches,[63] other spectroscopic methods [62], as well as experimental validations via mutagenesis. Finally, it should be noted that the dynamic networks of residues reported by the SyncDyn maps are underestimated as it depends on the number of NMR probes available and the window of motion analyzed, *i.e.*, residues manifesting relaxation dispersion. A possible solution is to expand our analysis to other range of motion using $T_{1\rho}$ measurements [3] or adiabatic relaxation dispersion experiments.[64, 65]

Enzyme function involves both structural and dynamical changes in the biomacromolecular matrix. The analysis of ligand titrations on protein fingerprints has been instrumental in characterizing orthosteric and allosteric effects in proteins.[66] Also, chemical shifts of both backbone amide and methyl-group side chains can be used to describe conformational shifts upon ligand binding [67] and identify networks of distally connected residues.[68-73]. The SyncDyn maps complement these approaches to fully characterize the structural and dynamic response to ligand binding. The synchronicity of motions adds another layer of complexity to global and sub-global motions, though it is not universally applicable to all systems. However, as we gain access to dynamic

data on larger biomacromolecules, it will be intriguing to determine whether synchronous motions play a role in biological activity and whether they are a common characteristic of cooperative systems. Additionally, this approach could be useful for exploring the organization of long-range dynamics in intrinsically disordered proteins [74] and polypeptides that exhibit multiple conformational states. and polypeptides with multiple conformational states.[75-77]

In conclusion, we present a method to identify networks of residues that fluctuate with similar frequencies (synchronous) that may mediate allostery in certain proteins. Our method largely removes experimenter bias at the early stages of relaxation dispersion analysis and will allow a standardized protocol for assessment of important protein motions. This approach provides 2D correlation maps that, when integrated with chemical shift covariance (CHESCA) maps for fast exchanging systems, offer structural and dynamic canvas as a starting point to interrogate allosteric phenomena in proteins and to guide future enzyme engineering or drug discovery efforts.

MATERIAL AND METHODS

Synthetic Data Generation

Using Matlab®, we generated ^{15}N CPMG relaxation dispersion data for a synthetic twenty-amino-acid peptide, using the Bloch McConnell equations. We created two clusters each consisting of six residues that share the same kinetic parameters. Cluster 1 with $k_f = 25 \text{ s}^{-1}$, $k_r = 500 \text{ s}^{-1}$, $\Delta\omega = 1 \text{ ppm}$, and $R_{20} = 10 \text{ s}^{-1}$; and Cluster 2 with $k_f = 100 \text{ s}^{-1}$, $k_r = 2000 \text{ s}^{-1}$, $\Delta\omega = 1 \text{ ppm}$, and $R_{20} = 10 \text{ s}^{-1}$. The data were generated for two magnetic fields with ^1H Larmor frequencies of 600 and 800 MHz. We set the T_{CPMG} at 20 ms and generated synthetic data for $\nu_{\text{CPMG}} = 50, 100, 150, 200, 250, 300, 350, 400, 500, 600, 700, 800, 900, \text{ and } 1000 \text{ s}^{-1}$ in which ν_{CPMG} is the rate at which π pulses are applied during the constant time relaxation, T_{CPMG} . Finally, we included 5% random noise into each dispersion profile. For the remaining residues, we randomly assigned values for k_f and k_r within a range of 0 to 5000 s^{-1} .

NMR Spectroscopy

The ^{13}C -ILV labeled catalytic subunit of protein kinase A (PKA-C) was expressed and purified as previously described.[22] Methyl-TROSY relaxation dispersion data, previously published,[22] were acquired on a 230 μM PKA-C sample at two magnetic fields (16.4 T and 19.97 T) using a constant relaxation time of 40 ms and inter-pulse delays frequencies $\nu_{\text{CPMG}} = 50 (\times 2), 100, 150, 200, 250, 300, 400, 500 (\times 2), 600, 800, 1000 (\times 2) \text{ s}^{-1}$. All the experiments were carried out at 300 K. The spectra were acquired in interleaved mode as a pseudo-3D with two-dimensional planes of 80 x 1024 complex points. The peak intensities were extracted using the FuDA (<https://www.ucl.ac.uk/hansen-lab/fuda/>).

For the RNase A, experimental CPMG relaxation dispersion data, published previously,[50] were acquired at static magnetic fields of 11.7, 14.1, and 18.8 T on a 773 μM ^{15}N -labeled T17A RNase A mutant and a 600 μM ^{15}N -labeled wild-type (WT) RNase A sample at pH = 6.4 and 298 K expressed and purified as previously described.[47, 49] The NMR relaxation data were typically acquired with spectral widths in the t_1 and t_2 dimensions of 2700 and 10000 Hz with a digital resolution of 0.1 and 0.2 points/Hz respectively. The proton carrier frequency was set to the H_2O resonance, and the ^{15}N frequency was placed in the middle of the amide region at 120 ppm. Spin-relaxation rate constants at each CPMG pulse repetition time (τ_{cp}) were acquired using a constant time [78] total relaxation delay of 40 ms. Transverse relaxation rates were determined for CPMG frequencies $\nu_{\text{CPMG}} = 50, 100, 150, 200 (\times 2), 250, 300, 400, 500, 700 (\times 2), 800 \text{ s}^{-1}$. The individual spectra were acquired as an interleaved three-dimensional experiment in which the two-dimensional planes were extracted, and peak intensities were determined from a 3 x 3 grid using in-house written software.

Data Analysis (SyncDyn maps)

To build the SyncDyn maps for PKA-C, we analyzed the relaxation dispersion data collected at 700 and 850 MHz for 102 methyl groups. A total of 5151 residue pairs were fitted with the Broyden-Fletcher-Goldfarb-Shanno (BFGS) algorithm [79] using an in-house Python script. For RNase A, we analyzed the relaxation dispersion data of 163 amide groups measured at 600, 700, and 800 MHz. A total number of 13203 residue pairs were fitted. The total computational time required for pair-fitting the CPMG-RD curves for all possible pairs was ~10 minutes on a PC with an Intel 12th generation i9 processor.

CRedit authorship contribution statement

Manu V.S.: Methodology, Investigation, Conceptualization, Formal analysis, Writing – original draft. **Giuseppe Melacini:** Conceptualization, Writing – original draft. **Evgenii L. Kovrigin:** Conceptualization Writing – review & editing. **Patrick J. Loria:** Conceptualization Writing – review & editing. **Gianluigi Veglia:** Conceptualization, Formal analysis, Funding acquisition, Writing – original draft, review & editing.

DECLARATION OF COMPETING INTEREST

The authors declare no competing financial interests or personal relationships that could influence the work reported in this paper.

ACKNOWLEDGMENTS

G.V. was supported by the National Institute of Health (CA290129) and by U.S. National Science Foundation (CHE-2304829). J.P.L was supported by NIH GM106121, CA281044, and NSF MCB2412821. G.M. was supported by funding provided by the Canadian Institutes of Health

Research Grant 389522 and 186329, and the Natural Sciences and Engineering Research Council of Canada Grant RGPIN-2019-05990.

Appendix A. Supplementary data

Supplementary data to this article can be found online at [XXXXXXXXXX](#)

REFERENCES

- [1] A. Sekhar, L.E. Kay, An NMR View of Protein Dynamics in Health and Disease, *Annu Rev Biophys*, 48 (2019) 297-319.
- [2] D.D. Boehr, H.J. Dyson, P.E. Wright, An NMR perspective on enzyme dynamics, *Chem Rev*, 106 (2006) 3055-3079.
- [3] A.G. Palmer, 3rd, C.D. Kroenke, J.P. Loria, Nuclear magnetic resonance methods for quantifying microsecond-to-millisecond motions in biological macromolecules, *Methods Enzymol*, 339 (2001) 204-238.
- [4] A.J. Wand, Dynamic activation of protein function: a view emerging from NMR spectroscopy, *Nat Struct Biol*, 8 (2001) 926-931.
- [5] S.R. Tzeng, C.G. Kalodimos, Protein dynamics and allostery: an NMR view, *Curr Opin Struct Biol*, 21 (2011) 62-67.
- [6] K. Henzler-Wildman, D. Kern, Dynamic personalities of proteins, *Nature*, 450 (2007) 964-972.
- [7] J. Monod, J. Wyman, J.P. Changeux, On the Nature of Allosteric Transitions: A Plausible Model, *J Mol Biol*, 12 (1965) 88-118.
- [8] D.E. Koshland, Jr., G. Nemethy, D. Filmer, Comparison of experimental binding data and theoretical models in proteins containing subunits, *Biochemistry*, 5 (1966) 365-385.
- [9] J.P. Changeux, 50 years of allosteric interactions: the twists and turns of the models, *Nat Rev Mol Cell Biol*, 14 (2013) 819-829.
- [10] S.J. Wodak, E. Paci, N.V. Dokholyan, I.N. Berezovsky, A. Horovitz, J. Li, V.J. Hilser, I. Bahar, J. Karanicolas, G. Stock, P. Hamm, R.H. Stote, J. Eberhardt, Y. Chebaro, A. Dejaegere, M. Cecchini, J.P. Changeux, P.G. Bolhuis, J. Vreede, P. Faccioli, S. Orioli, R. Ravasio, L. Yan, C. Brito, M. Wyart, P. Gkeka, I. Rivalta, G. Palermo, J.A. McCammon, J. Panecka-Hofman, R.C. Wade, A. Di Pizio, M.Y. Niv, R. Nussinov, C.J. Tsai, H. Jang, D. Padhorny, D. Kozakov, T. McLeish, Allostery in Its Many Disguises: From Theory to Applications, *Structure*, 27 (2019) 566-578.
- [11] Q. Cui, M. Karplus, Allostery and cooperativity revisited, *Protein Sci*, 17 (2008) 1295-1307.
- [12] B.F. Volkman, D. Lipson, D.E. Wemmer, D. Kern, Two-state allosteric behavior in a single-domain signaling protein, *Science*, 291 (2001) 2429-2433.
- [13] J.F. Swain, L.M. Gierasch, The changing landscape of protein allostery, *Curr Opin Struct Biol*, 16 (2006) 102-108.
- [14] R. Nussinov, C.J. Tsai, Allostery in disease and in drug discovery, *Cell*, 153 (2013) 293-305.
- [15] S. Gianni, P. Jemth, Allostery Frustrates the Experimentalist, *J Mol Biol*, 435 (2023) 167934.
- [16] G.P. Lisi, J.P. Loria, Solution NMR Spectroscopy for the Study of Enzyme Allostery, *Chem Rev*, (2016).

- [17] S. Grutsch, S. Bruschweiler, M. Tollinger, NMR Methods to Study Dynamic Allostery, *Plos Comput Biol*, 12 (2016) e1004620.
- [18] K.W. East, E. Skeens, J.Y. Cui, H.B. Belato, B. Mitchell, R. Hsu, V.S. Batista, G. Palermo, G.P. Lisi, NMR and computational methods for molecular resolution of allosteric pathways in enzyme complexes, *Biophys Rev*, 12 (2020) 155-174.
- [19] T.R. Alderson, L.E. Kay, Unveiling invisible protein states with NMR spectroscopy, *Curr Opin Struct Biol*, 60 (2020) 39-49.
- [20] H.Y. Carr, E.M. Purcell, Effects of Diffusion on Free Precession in Nuclear Magnetic Resonance Experiments, *Phys Rev*, 94 (1954) 630-638.
- [21] S. Meiboom, D. Gill, Modified Spin-Echo Method for Measuring Nuclear Relaxation Times, *Rev Sci Instrum*, 29 (1958) 688-691.
- [22] Y. Wang, M. V.S. J. Kim, G. Li, L.G. Ahuja, P. Aoto, S.S. Taylor, G. Veglia, Globally correlated conformational entropy underlies positive and negative cooperativity in a kinase's enzymatic cycle, *Nature Communications*, 10 (2019) 799.
- [23] H.M. McConnell, Reaction Rates by Nuclear Magnetic Resonance, *J Chem Phys*, 28 (1958) 430-431.
- [24] S. Weisberg, *Applied Linear Regression*, Wiley series in probability and statistics, Wiley, 2014.
- [25] E.L. Kovrigin, J.G. Kempf, M.J. Grey, J.P. Loria, Faithful estimation of dynamics parameters from CPMG relaxation dispersion measurements, *J Magn Reson*, 180 (2006) 93-104.
- [26] R.E. Turnham, J.D. Scott, Protein kinase A catalytic subunit isoform PRKACA; History, function and physiology, *Gene*, 577 (2016) 101-108.
- [27] S.S. Taylor, F.W. Herberg, G. Veglia, J. Wu, Edmond Fischer's kinase legacy: History of the protein kinase inhibitor and protein kinase A, *IUBMB Life*, 75 (2023) 311-323.
- [28] D. Gagne, N. Doucet, Structural and functional importance of local and global conformational fluctuations in the RNase A superfamily, *FEBS J*, 280 (2013) 5596-5607.
- [29] L.R. Masterson, C. Cheng, T. Yu, M. Tonelli, A. Kornev, S.S. Taylor, G. Veglia, Dynamics connect substrate recognition to catalysis in protein kinase A, *Nat Chem Biol*, 6 (2010) 821-828.
- [30] L.R. Masterson, A. Mascioni, N.J. Traaseth, S.S. Taylor, G. Veglia, Allosteric cooperativity in protein kinase A, *Proc Natl Acad Sci U S A*, 105 (2008) 506-511.
- [31] J. Kim, L.G. Ahuja, F.A. Chao, Y. Xia, C.L. McClendon, A.P. Kornev, S.S. Taylor, G. Veglia, A dynamic hydrophobic core orchestrates allostery in protein kinases, *Sci Adv*, 3 (2017) e1600663.
- [32] D.A. Johnson, P. Akamine, E. Radzio-Andzelm, M. Madhusudan, S.S. Taylor, Dynamics of cAMP-dependent protein kinase, *Chem Rev*, 101 (2001) 2243-2270.
- [33] J. Kim, G. Li, M.A. Walters, S.S. Taylor, G. Veglia, Uncoupling Catalytic and Binding Functions in the Cyclic AMP-Dependent Protein Kinase A, *Structure*, 24 (2016) 353-363.
- [34] J.A. Adams, Kinetic and catalytic mechanisms of protein kinases, *Chem Rev*, 101 (2001) 2271-2290.
- [35] L.R. Masterson, L. Shi, E. Metcalfe, J. Gao, S.S. Taylor, G. Veglia, Dynamically committed, uncommitted, and quenched states encoded in protein kinase A revealed by NMR spectroscopy, *Proc Natl Acad Sci U S A*, 108 (2011) 6969-6974.
- [36] A.K. Srivastava, L.R. McDonald, A. Cembran, J. Kim, L.R. Masterson, C.L. McClendon, S.S. Taylor, G. Veglia, Synchronous Opening and Closing Motions Are Essential for cAMP-Dependent Protein Kinase A Signaling, *Structure*, 22 (2014) 1735-1743.
- [37] L.F. Ten Eyck, S.S. Taylor, A.P. Kornev, Conserved spatial patterns across the protein kinase family, *Biochim Biophys Acta*, 1784 (2008) 238-243.
- [38] A.P. Kornev, S.S. Taylor, Defining the conserved internal architecture of a protein kinase, *Biochim Biophys Acta*, 1804 (2010) 440-444.
- [39] C. Olivieri, G.C. Li, Y. Wang, S.M. V, C. Walker, J. Kim, C. Camilloni, A. De Simone, M. Vendruscolo, D.A. Bernlohr, S.S. Taylor, G. Veglia, ATP-competitive inhibitors modulate the substrate binding cooperativity of a kinase by altering its conformational entropy, *Sci Adv*, 8 (2022) eabo0696.

- [40] S.R. Tzeng, C.G. Kalodimos, Allosteric inhibition through suppression of transient conformational states, *Nat Chem Biol*, 9 (2013) 462-465.
- [41] I.R. Kleckner, M.P. Foster, GUARDD: user-friendly MATLAB software for rigorous analysis of CPMG RD NMR data, *J Biomol NMR*, 52 (2012) 11-22.
- [42] C. Walker, Y. Wang, C. Olivieri, S.M. V, J. Gao, D.A. Bernlohr, D. Calebiro, S.S. Taylor, G. Veglia, Is Disrupted Nucleotide-Substrate Cooperativity a Common Trait for Cushing's Syndrome Driving Mutations of Protein Kinase A?, *J Mol Biol*, 433 (2021) 167123.
- [43] C. Walker, Y. Wang, C. Olivieri, A. Karamafrooz, J. Casby, K. Bathon, D. Calebiro, J. Gao, D.A. Bernlohr, S.S. Taylor, G. Veglia, Cushing's syndrome driver mutation disrupts protein kinase A allosteric network, altering both regulation and substrate specificity, *Science Advances*, 5 (2019) eaaw9298.
- [44] C. Olivieri, C. Walker, A. Karamafrooz, Y. Wang, V.S. Manu, F. Porcelli, D.K. Blumenthal, D.D. Thomas, D.A. Bernlohr, S.M. Simon, S.S. Taylor, G. Veglia, Defective internal allosteric network imparts dysfunctional ATP/substrate-binding cooperativity in oncogenic chimera of protein kinase A, *Commun Biol*, 4 (2021) 321.
- [45] R.E. Cathou, G.G. Hammes, Relaxation spectra of ribonuclease. 3. Further investigation of the interaction of ribonuclease and cytidine 3'-phosphate, *J Am Chem Soc*, 87 (1965) 4674-4680.
- [46] E.L. Kovrigin, R. Cole, J.P. Loria, Temperature dependence of the backbone dynamics of ribonuclease A in the ground state and bound to the inhibitor 5'-phosphothymidine (3'-5')pyrophosphate adenosine 3'-phosphate, *Biochemistry*, 42 (2003) 5279-5291.
- [47] R. Cole, J.P. Loria, Evidence for flexibility in the function of ribonuclease A, *Biochemistry*, 41 (2002) 6072-6081.
- [48] N. Doucet, E.D. Watt, J.P. Loria, The flexibility of a distant loop modulates active site motion and product release in ribonuclease A, *Biochemistry*, 48 (2009) 7160-7168.
- [49] N. Doucet, G. Khirich, E.L. Kovrigin, J.P. Loria, Alteration of hydrogen bonding in the vicinity of histidine 48 disrupts millisecond motions in RNase A, *Biochemistry*, 50 (2011) 1723-1730.
- [50] E.D. Watt, H. Shimada, E.L. Kovrigin, J.P. Loria, The mechanism of rate-limiting motions in enzyme function, *P Natl Acad Sci USA*, 104 (2007) 11981-11986.
- [51] A. Cooper, D.T. Dryden, Allostery without conformational change. A plausible model, *Eur Biophys J*, 11 (1984) 103-109.
- [52] A. Hacısuleyman, A. Erkip, B. Erman, B. Erman, Synchronous and Asynchronous Response in Dynamically Perturbed Proteins, *J Phys Chem B*, 125 (2021) 729-739.
- [53] Y. Bozkurt Varolgunes, A. Demir, ProteinAC: a frequency domain technique for analyzing protein dynamics, *Phys Biol*, 15 (2018) 026009.
- [54] T.R. Alderson, L.E. Kay, NMR spectroscopy captures the essential role of dynamics in regulating biomolecular function, *Cell*, 184 (2021) 577-595.
- [55] P.K. Agarwal, S.R. Billeter, P.T. Rajagopalan, S.J. Benkovic, S. Hammes-Schiffer, Network of coupled promoting motions in enzyme catalysis, *Proc Natl Acad Sci U S A*, 99 (2002) 2794-2799.
- [56] D.D. Boehr, D. McElheny, H.J. Dyson, P.E. Wright, The dynamic energy landscape of dihydrofolate reductase catalysis, *Science*, 313 (2006) 1638-1642.
- [57] P. Ojeda-May, A.U. Mushtaq, P. Rogne, A. Verma, V. Ovchinnikov, C. Grundstrom, B. Dulko-Smith, U.H. Sauer, M. Wolf-Watz, K. Nam, Dynamic Connection between Enzymatic Catalysis and Collective Protein Motions, *Biochemistry*, 60 (2021) 2246-2258.
- [58] D. Kern, E.R.P. Zuiderweg, The role of dynamics in allosteric regulation, *Current Opinion in Structural Biology*, 13 (2003) 748-757.
- [59] K.A. Henzler-Wildman, V. Thai, M. Lei, M. Ott, M. Wolf-Watz, T. Fenn, E. Pozharski, M.A. Wilson, G.A. Petsko, M. Karplus, C.G. Hubner, D. Kern, Intrinsic motions along an enzymatic reaction trajectory, *Nature*, 450 (2007) 838-844.

- [60] K.A. Henzler-Wildman, M. Lei, V. Thai, S.J. Kerns, M. Karplus, D. Kern, A hierarchy of timescales in protein dynamics is linked to enzyme catalysis, *Nature*, 450 (2007) 913-U927.
- [61] I.R. Kleckner, M.P. Foster, An introduction to NMR-based approaches for measuring protein dynamics, *Biochim Biophys Acta*, 1814 (2011) 942-968.
- [62] D. Xu, S.P. Meisburger, N. Ando, Correlated Motions in Structural Biology, *Biochemistry*, 60 (2021) 2331-2340.
- [63] M. Karplus, J. Kuriyan, Molecular dynamics and protein function, *Proc Natl Acad Sci U S A*, 102 (2005) 6679-6685.
- [64] N.J. Traaseth, F.A. Chao, L.R. Masterson, S. Mangia, M. Garwood, S. Michaeli, B. Seelig, G. Veglia, Heteronuclear Adiabatic Relaxation Dispersion (HARD) for quantitative analysis of conformational dynamics in proteins, *J Magn Reson*, 219 (2012) 75-82.
- [65] F.A. Chao, D. Khago, R.A. Byrd, Achieving pure spin effects by artifact suppression in methyl adiabatic relaxation experiments, *J Biomol NMR*, 74 (2020) 223-228.
- [66] M.P. Williamson, Using chemical shift perturbation to characterise ligand binding, *Prog Nucl Magn Reson Spectrosc*, 73 (2013) 1-16.
- [67] A. Cembran, J. Kim, J. Gao, G. Veglia, NMR mapping of protein conformational landscapes using coordinated behavior of chemical shifts upon ligand binding, *Phys Chem Chem Phys*, 16 (2014) 6508-6518.
- [68] R. Selvaratnam, S. Chowdhury, B. VanSchouwen, G. Melacini, Mapping allostery through the covariance analysis of NMR chemical shifts, *Proc Natl Acad Sci U S A*, 108 (2011) 6133-6138.
- [69] J.A. Byun, G. Melacini, NMR methods to dissect the molecular mechanisms of disease-related mutations (DRMs): Understanding how DRMs remodel functional free energy landscapes, *Methods*, 148 (2018) 19-27.
- [70] S. Boulton, R. Selvaratnam, R. Ahmed, G. Melacini, Implementation of the NMR CHEMical Shift Covariance Analysis (CHESCA): A Chemical Biologist's Approach to Allostery, *Methods Mol Biol*, 1688 (2018) 391-405.
- [71] R. Ahmed, M. Akcan, A. Khondker, M.C. Rheinstadter, J.C. Bozelli, Jr., R.M. Epand, V. Huynh, R.G. Wylie, S. Boulton, J. Huang, C.P. Verschoor, G. Melacini, Atomic resolution map of the soluble amyloid beta assembly toxic surfaces, *Chem Sci*, 10 (2019) 6072-6082.
- [72] R. Ahmed, J. Huang, M. Akimoto, T. Shi, G. Melacini, Atomic Resolution Map of Hierarchical Self-Assembly for an Amyloidogenic Protein Probed through Thermal (15)N-R(2) Correlation Matrices, *J Am Chem Soc*, 143 (2021) 4668-4679.
- [73] J. Wang, A. Jain, L.R. McDonald, C. Gambogi, A.L. Lee, N.V. Dokholyan, Mapping allosteric communications within individual proteins, *Nat Commun*, 11 (2020) 3862.
- [74] G. Parigi, N. Rezaei-Ghaleh, A. Giachetti, S. Becker, C. Fernandez, M. Blackledge, C. Griesinger, M. Zweckstetter, C. Luchinat, Long-range correlated dynamics in intrinsically disordered proteins, *Journal of the American Chemical Society*, 136 (2014) 16201-16209.
- [75] C. Olivieri, Y. Wang, G.C. Li, S.M. V, J. Kim, B.R. Stultz, M. Neibergall, F. Porcelli, J.M. Muretta, D.D. Thomas, J. Gao, D.K. Blumenthal, S.S. Taylor, G. Veglia, Multi-state recognition pathway of the intrinsically disordered protein kinase inhibitor by protein kinase A, *Elife*, 9 (2020).
- [76] C.A. MacRaid, M. Zachrdla, D. Andrew, B. Krishnarjuna, J. Novacek, L. Zidek, V. Sklenar, J.S. Richards, J.G. Beeson, R.F. Anders, R.S. Norton, Conformational dynamics and antigenicity in the disordered malaria antigen merozoite surface protein 2, *PLoS One*, 10 (2015) e0119899.
- [77] B. Krishnarjuna, T. Sugiki, R.A.V. Morales, J. Seow, T. Fujiwara, K.L. Wilde, R.S. Norton, C.A. MacRaid, Transient antibody-antigen interactions mediate the strain-specific recognition of a conserved malaria epitope, *Commun Biol*, 1 (2018) 58.
- [78] F.A. Mulder, N.R. Skrynnikov, B. Hon, F.W. Dahlquist, L.E. Kay, Measurement of slow (micros-ms) time scale dynamics in protein side chains by (15)N relaxation dispersion NMR spectroscopy: application to Asn and Gln residues in a cavity mutant of T4 lysozyme, *J Am Chem Soc*, 123 (2001) 967-975.

[79] C.T. Kelley, Iterative methods for optimization., Society for Industrial and Applied Mathematics 1999.

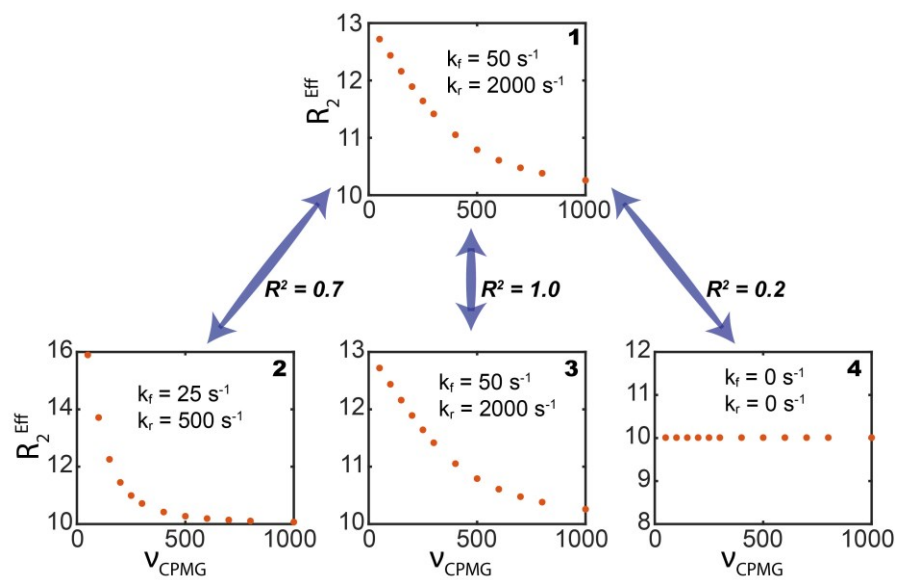


Figure 1. Pairing residues with synchronous motion. Simulated relaxation dispersion curves for sites undergoing chemical exchange on different time scales. The calculated R-squared values greater than 0.9 indicate similar k_f and k_r values (synchronous motion) for a given residue pair.

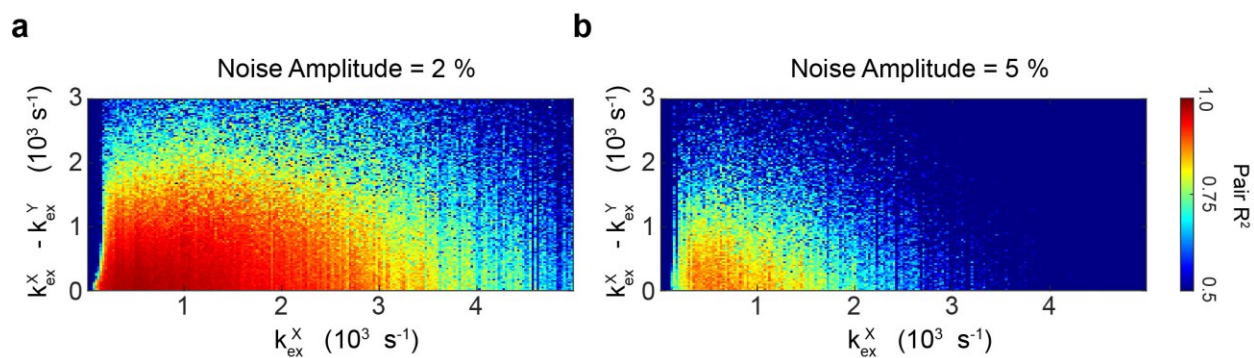


Figure 2. Simulated response of R-squared to exchange rates for two noise amplitudes. CPMG dispersion profiles simulated for two residues, X and Y, in exchange with their respective minor states X' and Y'. The populations of the minor states for the two species were set to $p(X') = p(Y') = 0.02$. The exchange rates for X and Y were k_{ex}^X and k_{ex}^Y , respectively. The simulations were performed for ^{15}N with $\Delta\omega = 1$ ppm. A pair fit was performed on X and Y for 200 x 120 different combinations of k_{ex}^X values ranging from 0 to 5000 s^{-1} and ($\Delta k_{ex} = k_{ex}^X - k_{ex}^Y$ ranging from 0 to 3000 s^{-1}). The response was simulated with noise amplitudes of 2% (a) and 5% (b) of the intrinsic relaxation rate ($R_2^0 = 10 \text{ s}^{-1}$).

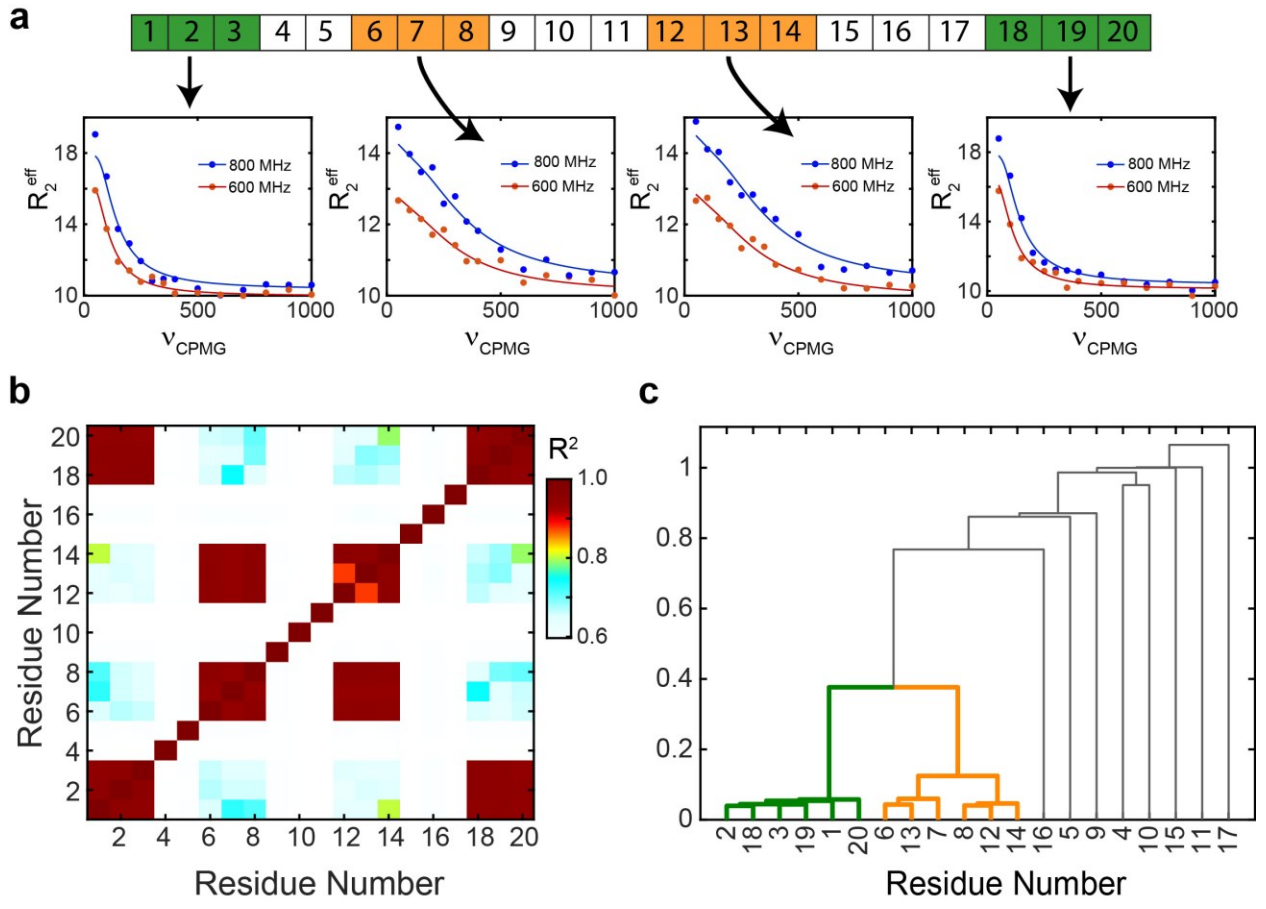


Figure 3. Simulated SyncDyn analysis of a synthetic twenty amino acid peptide. (a) Peptide sequence and selected dispersion profiles for two clusters of residues: cluster 1 (green) with $k_f = 25 \text{ s}^{-1}$, $k_r = 500 \text{ s}^{-1}$, $\Delta\omega = 1\text{ppm}$, $R_2^0 = 10 \text{ s}^{-1}$, and cluster 2 (orange) with $k_f = 100 \text{ s}^{-1}$, $k_r = 2000 \text{ s}^{-1}$, $\Delta\omega = 1\text{ppm}$, $R_2^0 = 10 \text{ s}^{-1}$. A 5% random noise was added to the dispersion profiles. Random values of k_f and k_r in the range of 0 to 5000 s^{-1} were assigned to the other residues. (b) Calculated SyncDyn map for the twenty amino acid peptide reveals high correlations (i.e., R -squared > 0.9) among residues 1-3, 18-20 and 6-8, and 12-14. (c) Dendrogram of the SyncDyn matrix revealing the highly correlated residue clusters.

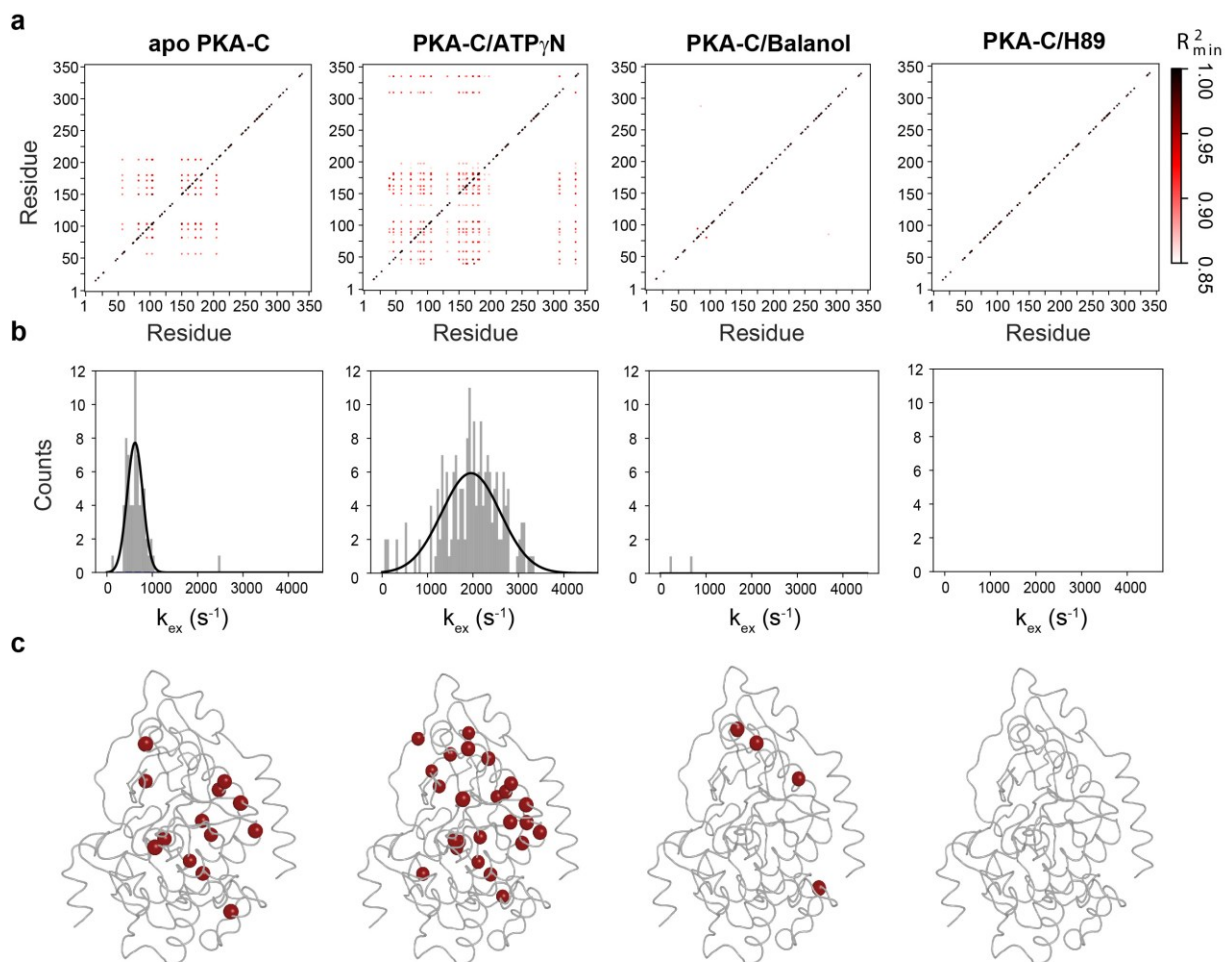


Figure 4. SyncDyn maps for different ligated forms of PKA-C. (a) SyncDyn maps for the apo, ATP γ N-bound, balanol-bound, and H89-bound PKA-C. (b) Distribution of the exchange rates for the different forms of PKA-C. Note that the area under each distribution is normalized relative to the largest area of the PKA-C/ATP γ N complex. (c) Mapping residue pairs with a R-squared values ≥ 0.85 on the X-ray structure of PKA-C (1ATP). ATP and PKI peptide are omitted for clarity.

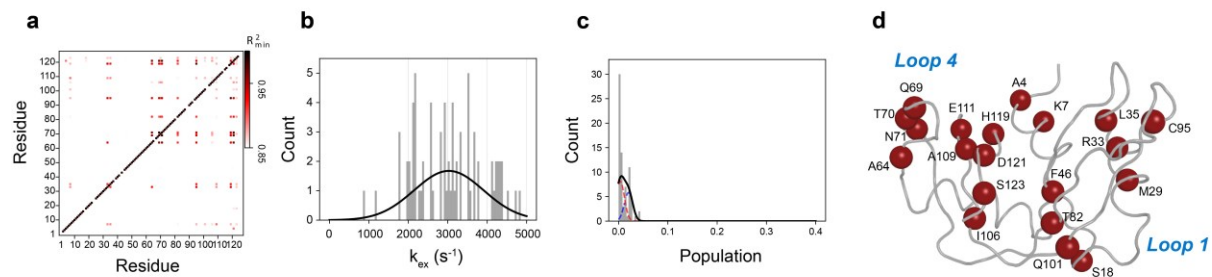


Figure 5. SyncDyn map of the T17A mutant of RNase A. (a) SyncDyn map of the T17A mutant of RNase using a R-squared ≥ 0.85 . (b) Normalized distribution of the exchange rates obtained from fitting the CPMG dispersion curves. (c) Distribution of the population of the conformational excited states. (d) Plot of the SyncDyn matrix of residue pairs with R-squared ≥ 0.85 .